Computational Fluid Dynamics JOURNAL vol.6 no.3 October 1997 (pp.325–340)

NUMERICAL ANALYSIS OF THREE-DIMENSIONAL TURBULENT STRUCTURE IN A TRAPEZOIDAL MEANDERING CHANNEL

Hitoshi SUGIYAMA Mitsunobu AKIYAMA Masayuki KAMEZAWA
Mieko TANAKA

Abstract

Numerical study of turbulent flow developing in meandering open-channel flow with trapezoidal cross section has been carried out by using algebraic stress model and boundary fitted coordinate system. The flow configuration of interest to this study consists of five meanders of trapezoidal cross section. In the calculation, governing equations are transformed from the physical plane to the calculation plane by boundary fitted coordinate system. Calculated results are compared with the experimental results available. As a result of this numerical study, it is found that the present method can predict well the characteristic features of the streamwise velocity, i.e., the maximum streamwise velocity occurs near inner bank at the bend apex and the position of the maximum velocity moves cross over section along the meandering channel which is different from those of curved open-channel flow. The calculated results of secondary flow show complex behavior due to imbalance between centrifugal force and pressure gradient as well as the experimental results. The distributions of turbulent energy, lateral and vertical shear stress are reproduced qualitatively by the present turbulent model. Moreover, invariants analysis has been performed by using calculated results in order to examine turbulent structure in meandering channel.

1 INTRODUCTION

Meandering flow which is composed by the several curved channel is typical flow as shown in natural rivers. In this meandering open-channel, the flow behavior is very complicated by the interaction between anisotropic turbulence near the free surface and centrifugal force generated by curved channel. A secondary flow initiated by the influence of curvature is well known and is be an important role on sediment transport in natural rivers. Therefore, the understanding of meandering channel flow is essential to design river system.

There are many studies on straight open-channel for inbank and overbank flow condition but a few research on meandering open-channel. Early work by Toebes and Sooky [1] identified some of flow characteristics in a multiple meandering channel by using Prandtl tube. They attempted to relate energy loss to observed internal flow structures associated with interaction between channel and floodplain flows. They concluded that the energy losses per unit length for the meandering channel were up to 2.5 times as large as for a uniform channel of the same width and for the same hydraulic radius and discharge and the energy loss in a meandering channel depended both Reynolds

Received on May 3, 1997.
Energy and Environmental Science,
Graduate School of Engineering,
Utsunomiya University,
2753 Ishii-cho, Utsunomiya, 321 Japan

and Froude number. Kiely [2] presented the distributions of longitudinal and secondary velocity using laser Doppler velocimeter in three different flood flow geometries. The measured data showed that the maximum streamwise velocities in the main channel were close to the inner bend and the direction of secondary flow was is anti-clockwise (looking downstream) with some magnitude as high as 30 % of the primary velocities in overbank flow. It is noted that this direction is opposite to that for inbank flow. Recently, the hydraulic behavior of compound meandering channel has been measured systematically by several researchers [3], [4], [5] based on the Flood Channel Facility at HR Wallingford. For example, Sellin, Ervine and Willetts [4] have obtained measured data involving velocity, surface level and discharge observations, employing three channel geometries, two floodplain widths, and a variety of floodplain roughness state. The influence of these conditions on the stage-discharge relationship has been presented and some deductions have been made from the velocity data about flow structures.

These experimental analysis are concerned with energy loss and prediction of discharge for meandering channel, while the development behavior of secondary flow and turbulent structure have been presented in detail by Shiono and Muto [6]. The distributions of the Reynolds stresses along the meandering channel and secondary flows were undertaken using laser Doppler velocimeter system in trapezoidal cross section meandering channel with straight floodpalin walls for bankfull and overbank flows. They clarified characteristic feature of meandering channel, for example, the maximum streamwise velocity occurs near the inner bank at the bend apex and moves crossing from the inner bank to the center at middle of cross section. At the same time, they emphasized that the measuring data including Reynolds stresses were instrumental in confirming the validation of turbulent model.

As a numerical analysis, Ervine and Ellis [7] have described the method for determining energy losses for the case of meandering channels with overbank flow and the method of sub-dividing the floodway for stage-discharge prediction. Greenhill and Sellin [8] also have presented the method to design compound meandering channels based on the Manning-Strickler equation. In the contrast with these method for predicting energy losses and discharge, to our knowledge, there is no report to analyze numerically three-dimensional meandering channel flow including Reynolds stresses.

From the review of these literature revealed that there is only a small experimental database including Reynolds stresses for meandering channel flow , Shiono and Muto [6] have measured the turbulent structure contained Reynolds stress components in detail. Recently, Muto et al. [9] have presented the turbulent structure and growth and decay prodesses of seconadry flow along meandering channels with rectangular cross section. Their experimental results are intended not only to provide insight into the physics of meandering channel flow, but also to serve as a basis for testing turbulent models applicable to this type of flow situation.

Considering from the review of literature, the main object is to predict the turbulent structure of meandering channel by using algebraic Reynolds stress model as a three-dimensional turbulent flow. In calculation, the boundary-fitted coordinate system is adopted in this study as the method of coordinate transformation. The calculated results are compared with the experimental data measured by Shiono and Muto [6] in order to examine the validity of the present method and to provide insight into the physics of meandering channel.

2 TECHNIQUE OF ANALYSIS

2.1 Subject of Numerical Analysis

In numerical analysis, the experimental data measured in detail by Shiono and Muto [6] was selected as a subject of calculation. They measured turbulent structures of meandering channel with inbank and overbank flow. In this study, the experimental data of meandering channel with inbank flow is adopted for comparison purpose. Figure 1 shows a schematic diagram of the experimental apparatus and the coordinate system set in meandering channel with trapezoidal cross section. Five meanders have been constructed with the following dimensions for one meander: bed width 16.5 cm, floodplain

height 5.3 cm and bend radius 42.5 cm with a vertical main channel wall, crossing over length 37.6 cm, meander one wave length 184.8 cm and a cross-over angle of 60 degree. In the five multiple meanders, a half meander wave length of the fourth meander section was used as a test section and was divided into 13 cross sections of which the turbulent measurements were undertaken at the 7 cross sections.

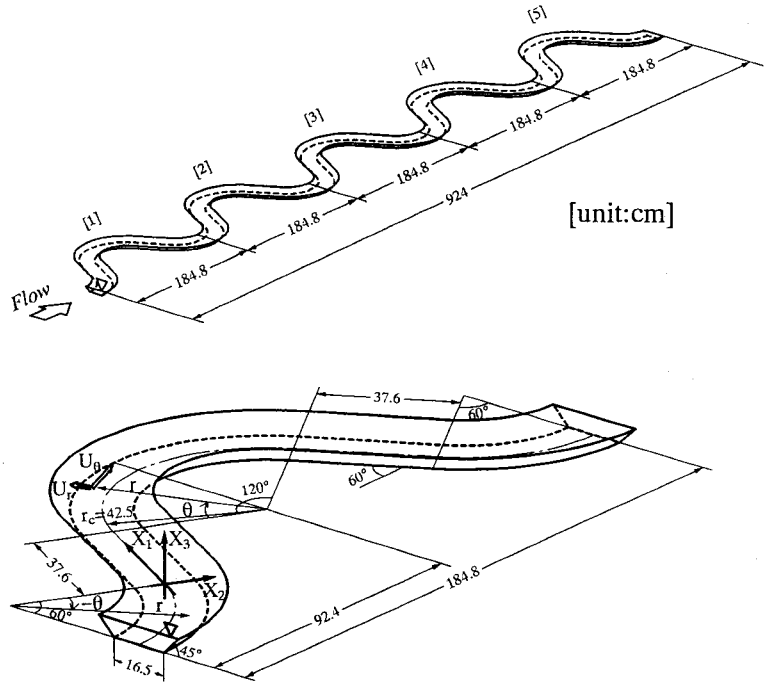

Fig.1: Meandering channel and definition of coordinate system

Cartesian coordinate and toroidal coordinate systems are applied in straight open-channel and meandering channel, respectively. The origin of Cartesian coordinate system lies at inlet section of straight open-channel as shown in figure 1. The upstream and downstream locations for straight open-channel represent positive sigh and negative sigh of turning angle θ,respectively. Therefore, turning angle $\theta = -60°$ are corresponded to inlet section of fourth meandering channel and $\theta = 60°$ is located at midway between inlet and outlet section of fourth meandering channel. In the experiment, Reynolds number evaluated on a axial bulk velocity U_b and hydraulic radius R was kept at $R_e = 4RU_b/ = 2.74 \times 10^4$

2.2 Governing Equations

The ensemble-averaged momentum equation is expressed as follows:

$$\frac{\partial \overline{U_i}}{\partial t} + \overline{U_k}\frac{\partial \overline{U_i}}{\partial x_k} = -\frac{1}{\rho}\frac{\partial \overline{P}}{\partial x_k} + \frac{\partial}{\partial x_k}(\nu\frac{\partial \overline{U_i}}{\partial x_k} - \overline{u_i u_j}) \tag{1}$$

where $\overline{(\,)}$ is the ensemble-averaged value. The correlations $\overline{u_i u_j}$ between fluctuating velocities which represent the Reynolds stresses appear in the momentum equations. The set of differential equations

governing the transport of the Reynolds stresses is derived from the Navier-Stokes equation as follows:

$$\frac{D\overline{u_iu_j}}{Dt} = -\left(\overline{u_iu_k}\frac{\partial \overline{U_j}}{\partial x_k} + \overline{u_ju_k}\frac{\partial \overline{U_i}}{\partial x_k}\right) + \overline{\frac{p}{\rho}\left(\frac{\partial u_i}{\partial x_j} + \frac{\partial u_j}{\partial x_i}\right)} - \frac{\partial}{\partial x_k}\left[\overline{u_iu_ju_k} - \nu\frac{\partial \overline{u_iu_j}}{\partial x_k} + \overline{\frac{p}{\rho}(\delta_{jk}u_i + \delta_{ik}u_j)}\right] - 2\nu\overline{\frac{\partial u_i}{\partial x_k}\frac{\partial u_j}{\partial x_k}} \tag{2}$$

The first term of the right hand side is the production term P_{ij}, the second term is the pressure strain correlation π_{ij}, the third term is the diffusion term $Diff_{,ij}$, and the forth term is the dissipation term. Adding to this, the first term of left hand side represents convection term. In the equation (1), the Reynolds stresses need to be simulated by a statistical turbulence model. In this study, algebraic Reynolds stress model is introduced to analyze anisotropic turbulence preciously. As regards the modeling of the convective and of the diffusion terms, the approximation by Rodi [10] was employed. By Rodi's approximation, these terms expressed in a differential form for Reynolds stress component can be transformed into the algebraic equation. The algebraic form is displayed as follows:

$$\frac{D\overline{u_iu_j}}{Dt} - Diff_{,ij} = \frac{\overline{u_iu_j}}{k}\left(\frac{Dk}{Dt} - Diff_{,k}\right) = \frac{\overline{u_iu_j}}{k}(P_k - \varepsilon) \tag{3}$$

$$P_k = -\overline{u_ku_l}\frac{\partial \overline{U_k}}{\partial x_l} \tag{4}$$

$Diff_{,ij}$, $Diff_{,k}$ and P_k denote the diffusion term of transport equation for Reynolds stresses, that of transport equation for turbulent energy and production term of transport equation for turbulent energy, respectively. In the Reynolds stress model, a particularly problematic task is the modeling of the pressure-strain correlation term which is important term to redistribute turbulent energy among Reynolds stresses. The pressure-strain term is shown in Table 1 and the constants used in this analysis are summarized in Table 2. Authors [11] described the derivation of pressure-strain term and its constants in detail. In Table 1, $f(L/X_w)$ is a function of the dimensionless wall distance. It expresses the influence of the wall and takes the value 1 in its vicinity, approaching 0 in with the increasing distance of it. X_w expresses the distance from the wall and L defined length scale of turbulence.

The turbulent energy k and dissipation ϵ are calculated from the following equations:

$$\frac{\partial k}{\partial t} + \overline{U_k}\frac{\partial k}{\partial x_k} = -\overline{u_iu_j}\frac{\partial \overline{U_k}}{\partial x_l} + \frac{\partial}{\partial x_k}\left[(\nu\delta_{kl} + c_s\frac{k}{\epsilon}\overline{u_ku_l})\frac{\partial k}{x_l}\right] - \epsilon \tag{5}$$

$$\frac{\partial \epsilon}{\partial t} + \overline{U_k}\frac{\partial \epsilon}{\partial x_k} = -c_{\epsilon 1}\frac{\epsilon}{k}\overline{u_iu_j}\frac{\partial \overline{U_k}}{\partial x_l} + \frac{\partial}{\partial x_k}\left[(\nu\delta_{kl} + c_\epsilon\frac{k}{\epsilon}\overline{u_ku_l})\frac{\partial \epsilon}{x_l}\right] - c_{\epsilon 2}\frac{\epsilon^2}{k} \tag{6}$$

where model constants are $c_s = 0.22, c_\epsilon = 0.18, c_{\epsilon 1} = 1.44$ and $c_{\epsilon 2} = 1.92$.

2.3 Boundary Condition at a Free Surface

Accurate prediction of turbulent structure is required not only elaborate turbulent model but also reasonable boundary condition at free surface.The free surface can be considered to a first approximation as a plane of symmetry under the absence of wind induced shear stress, i.e., a zero gradient is often used as the boundary condition for the velocity components and for the turbulent quantities at the free surface. However, the presence of a free surface reduces the length scale and, thus, increases the dissipation rate, as pointed out by Hunt [12]. Several researchers [13], [14] have proposed the

Table 1: Modeling of the pressure-strain correlation term

$\pi_{ij,1} + \pi_{ji,1}$	$-C_1 \frac{\varepsilon}{k}(\overline{u_i u_j} - \frac{2}{3}k\delta_{ij})$
$\pi_{ij,2} + \pi_{ji,2}$	$-\frac{C_2+8}{11}(P_{ij} - \frac{2}{3}P_k\delta_{ij}) + \zeta k(\frac{\partial U_i}{\partial x_j} + \frac{\partial U_j}{\partial x_i})$ $-\frac{8C_2-2}{11}(D_{ij} - \frac{2}{3}P_k\delta_{ij})$
$[\pi_{ij} + \pi_{ji}]_w$	$C_1 = C_1^* + C_1' f(\frac{L}{X_w})$ $C_2 = C_2^* + C_2' f(\frac{L}{X_w})$ $\zeta = \zeta^* + \zeta' f(\frac{L}{X_w})$
$P_{ij} = -\overline{u_i u_k}\frac{\partial U_j}{\partial x_k} - \overline{u_j u_k}\frac{\partial U_i}{\partial x_k}$ $D_{ij} = -\overline{u_i u_k}\frac{\partial U_k}{\partial x_j} - \overline{u_j u_k}\frac{\partial U_k}{\partial x_i}$ $P_k = -\overline{u_k u_l}\frac{\partial U_k}{\partial x_l}$ $f\left(\frac{L}{X_w}\right) = \frac{C_\mu^{\frac{3}{4}} k^{\frac{3}{2}}}{\kappa\ \varepsilon}\frac{1}{X_w}$	

Table 2: Constants in the pressure-strain correlation term

C_1^*	C_2^*	ζ^*	C_1'	C_2'	ζ'
1.4	0.44	-0.16	-0.35	0.12	-0.1

boundary condition at free surface taking account of adjustment with the turbulent model adopted in numerical analysis. In this study, considering the behavior of turbulent near free surface is physically similar to that of wall, the turbulent dissipation ϵ is defined as following equation:

$$\epsilon = \frac{c_\mu^{3/4} k^{3/2}}{\kappa y} \tag{7}$$

which is the same expression of wall function. In the above equation, y, κ and c_μ are the distance between the free surface and first calculated point, *Kármán's* constant and empirical constant,respectively.

Nakagawa, Nezu and Ueda [15] have investigated the hydraulic behavior near the free surface by making use of hot film anemometer. They have pointed out as the major important result that velocity fluctuation perpendicular to the free surface decreases with approaching the free surface. Its damping effect of velocity fluctuation is similar to that of near the wall. But the damping effect of velocity fluctuation in the vicinity of free surface is stronger than that of near wall, as presented experimentally by Nakagawa et al [15]. As a result of this damping effect, the intensity of velocity fluctuation perpendicular to the free surface displays a small value compared with that of velocity fluctuation near the wall before reaching the free surface. In order to realize the existence of this strong damping effect near the free surface, the value of velocity fluctuation perpendicular to the free surface sets to be zero at not only free surface but also the first grid point from the free surface as a

boundary condition. The validity of this treatment have been confirmed from the calculated results of straight open-channel flow calculated by Sugiyama et al [16].

2.4 Coordinate Transformation

Anisotropic turbulent model proves its worth when it is applied to the complicated turbulent flow. The complicated turbulent flow is generally observed in complicated configuration flume. Therefore, the coordinate transformation is indispensable to set boundary conditions preciously along the boundary. In this research, boundary-fitted coordinate system (BFC) was adopted as the coordinate transformation. The transformation of the governing equations to the calculation level is accomplished according to following mathematical definitions:

$$\frac{\partial}{\partial X_i} = \frac{\partial \xi}{\partial X_i}\frac{\partial}{\partial \xi} + \frac{\partial \eta}{\partial X_i}\frac{\partial}{\partial \eta} + \frac{\partial \zeta}{\partial X_i}\frac{\partial}{\partial \zeta} \tag{8}$$

The procedure of the transformation of the governing equations has been described in detail by the author's other report [17].

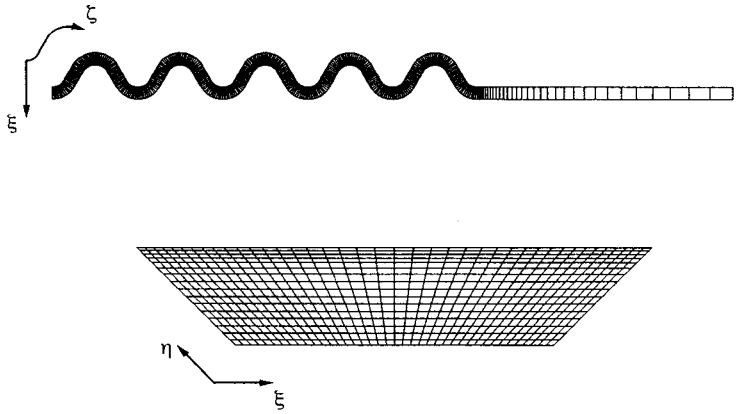

Fig.2: Arrangement of calculation mesh

2.5 Numerical Analysis

Numerical analysis has been carried out three-dimensional meandering channel included five meanders as shown in figure 1. But, in calculation, downstream straight tangent of $156.6R(R = 3.5cm)$ with trapezoidal cross section were used to set Neumann condition at outlet section. Figure 2 shows the layout of the calculation mesh over meandering channel. In this figure, ξ, η and ζ are identified as the coordinate axes along the numerical grids. Numerical grids are located finely near the free surface and walls where the variation of physical parameters are observed. Numerical grid with 372 nodes in the streamwise and with 41 × 17 over total cross section are generated in calculation. In curved channel, numerical grids are made every 5 degree. Reynolds number of calculation is determined by the experimental discharge ($Q = 2.251x10^{-3}m^3/s$), mean bulk velocity(U_b=0.207m/s) and trapezoidal shape as shown in figure 1. As a result of this procedure, Reynolds number became $R_e = 2.69 \times 10^4$ which is a little different from the experiment.

As for the inlet condition , the uniform streamwise velocity and the value of $k = U_b^2 \times 10^{-5}$ and $\epsilon = k^{3/2}/4R$ were adopted by assuming small fluctuating velocity at the channel inlet. The consistence

of the universal velocity distribution at the vicinity of the wall and also the supposition of the local equilibrium lead to the utilization of the law of the wall function as the boundary conditions for k and ϵ equations. The present turbulent model is classified as a high Reynolds number model, so that we made use of wall function method. Moreover, it is assumed that water depth is kept constant in the calculation, although variation of pressure makes water depth change along downstream in the experiment,

The governing equations are discretized by finite differential method with non-staggered computational grid. The QUICK(quadratic interpolation for convective kinematics) approximation of Leonard [18] is used for discretizing convective transport term and the other terms are discretized by central-difference scheme. Unsteady term of governing equation is discretized by implicit method, so that this implicit method impose the limitation that Courant number must be satisfied to be small than unit. Hence, time step is fixed as Courant number becomes smaller than unit in the calculation.

3 RESULTS AND CONSIDERATIONS

3.1 Comparison of Mean Flow Results

Streamwise mean flow are compared at the same cross section of the experiment as shown in figure 3. The value of counter lines is nondimensionalized by bulk velocity. In the case of negative sigh for θ, left and right sides of cross section represent inner and outer banks, respectively and in the case of positive sigh for θ, vise versa. At the inlet section $\theta = -60$ degree, the maximum streamwise velocity is produced near inner bank in both results. It is pointed out as a characteristic features in the experiment that the location of maximum velocity moves gradually from inner bank of inlet section $\theta = -60°$ to inner bank of outlet section $\theta = 60°$ as the flow develops. These phenomena can be also predicted well by the present method and is different from curved open-channel flow, i.e., generally, the location of maximum velocity is observed near outer bank in curved open- channel. Therefore, the maximum streamwise velocity of inner bank and the movement of maximum velocity are typical features in meandering channel flow.

Moreover, the existence of maximum velocity near inner bank is probably caused by the pressure gradient greater than centrifugal force. Considering from the experimental result [19] that the existence of maximum velocity near inner wall is also observed in meandering closed duct with square cross section, this phenomenon is not induced by the free surface but by the pressure gradient owing to meandering shape.

The movement of maximum velocity is intimately bound up with the secondary flow. Figure 4 shows the comparison of secondary flow looking downstream at the same cross section of streamwise velocity. At $\theta = -60°$, anti-clockwise vorticity and secondary flow from inner bank to outer bank are recognized near the central region and river bed region, respectively, in both results. The anti-clockwise vorticity prevents maximum velocity from moving towards outer bank. Compared distribution of $\theta = -60°$ with that of $\theta = 60°$ in both results, it is found that the distribution of $\theta = -60°$ looking downstream is coincident with that of $\theta = 60°$ looking upstream. At $\theta = -30°$ and $-0°$, the secondary flow is generated from inner bank to outer bank, which suggests that centrifugal force is superior to the force derived by pressure gradient.

In the straight open-channel between two curved channel, the magnitude of secondary flow decreases with decreasing centrifugal force and clockwise vorticity occupies in whole cross section. The present method is also able to predict these features but anti-clockwise vorticity near right bank of cross section is not reproduced clearly.

Entering into the second curved channel, the pressure gradient, which operates from high pressure side toward low pressure side, produces the secondary flow from outer bank to inner bank along river bed. In the experiment at $\theta = 0°$, secondary vector near $(r_c - r)/4R = -0.5$ rises up toward the free surface, while calculated results show the same behavior. At $\theta = 30°$ which is section of second

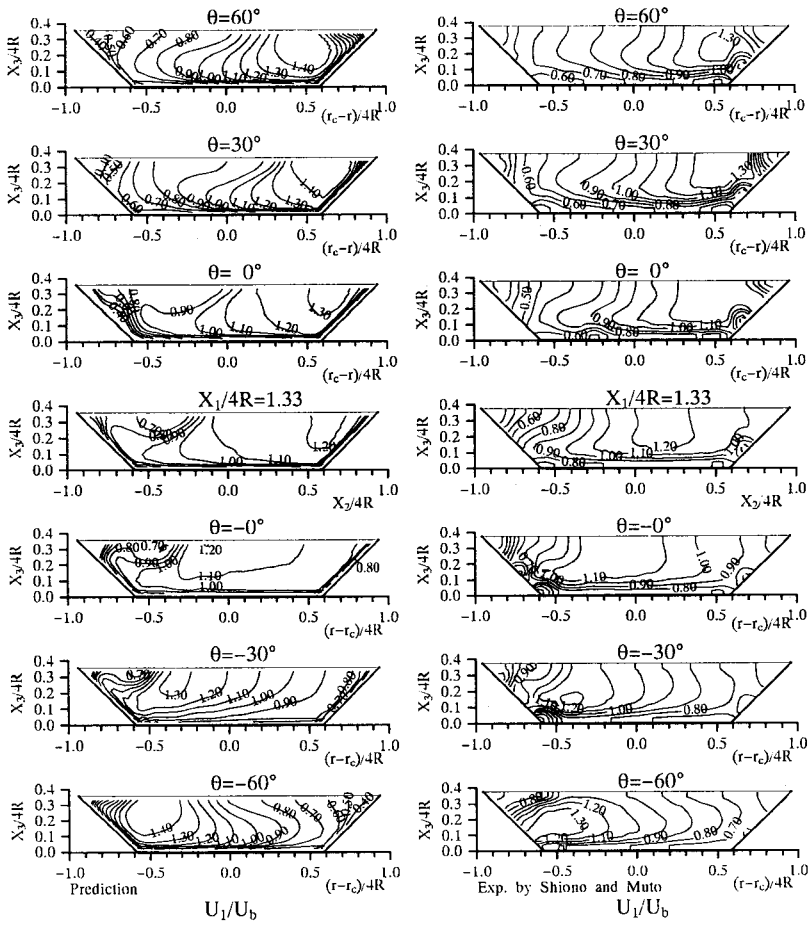

Fig.3: Comparison of streamwise mean velocity

curved channel, secondary vectors are more complicated by imbalance between pressure gradient and centrifugal force. Clockwise vorticity is observed in both results but the central location of clockwise vorticity is not predicted accurately by the present method. From the comparison between the experiment and the calculation, it is found that main features are reproduced well by the present method.

The magnitude of the secondary flow is compared with experiment as shown in figure 5. Streamwise vorticity ω_θ is normalized by bulk mean velocity U_b and hydraulic radius R. In the first curved channel, the calculated result of $\theta = -60°$ is in good agreement with the experiment. Adding to this, it is made clear as a discrepancy that distinct clockwise and anti-clockwise vorticity can be seen clearly at $\theta = -30°$ and $-0°$ in the experiment, while the calculated results of the same stations display the existence of clockwise vorticity judging from the zero value line does not lie in cross section. When particular attention is given to the magnitude near both banks, the calculated results suggest that high intensity of streamwise vorticity exists near the inner bank. This phenomenon can be also understood

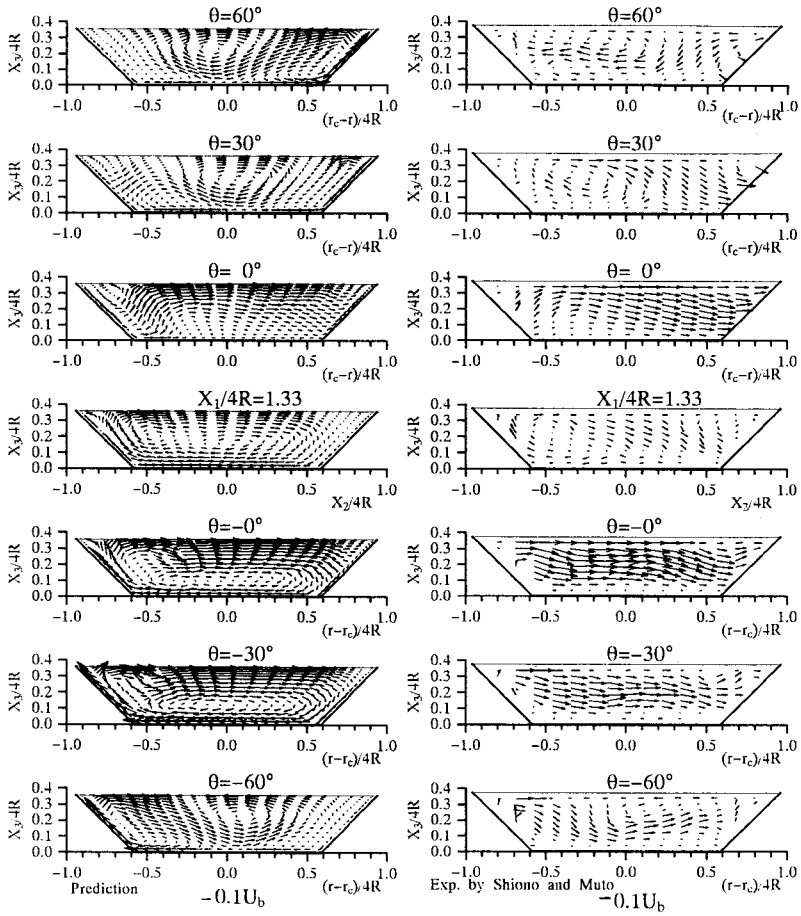

Fig.4: Comparison of secondary flow vectors

from the distributions of the secondary flow vectors in the calculation.

In the straight open channel at $X_1/4R = 1.33$, although an increase of positive sigh region and the appearance of zero value line near river bed are recognized as a common features in both results, the present method is not able to reproduce the zero isoline lying from the right hand side toward free surface. At this station, the intensity of vorticity decreases near the left side bank compared with that near inner bank in the first curved channel.

The calculated results in the second curved channel show a good agreement in the experiment in the light of the formation of zero value line. But the calculation has tendency to overpredict the experimental value in every stations. As for the intensity of vorticity of calculated results, the high value region is generated near the inner bank as the flow develops along downstream, so that the maximum absolute value is observed clearly near inner bank at $\theta = \pm 60°$, which phenomenon is not observed in the experiment. Considering this maximum intensity of streamwise vorticity near inner bank and the maximum streamwise velocity at same region, an erosion of the bank is promoted more

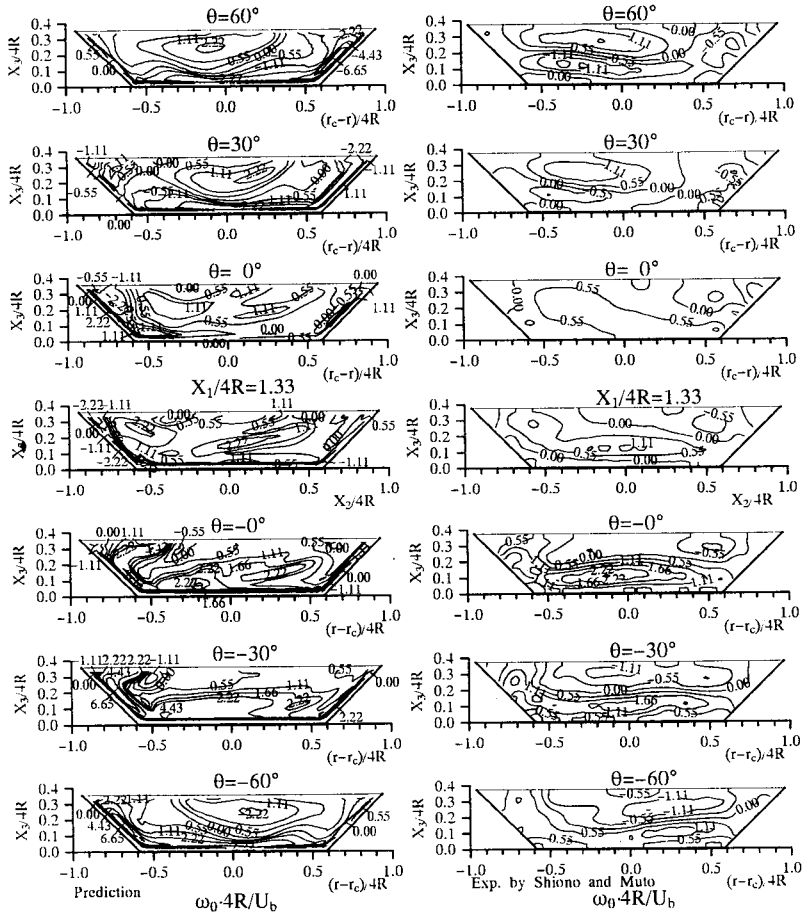

Fig.5: Comparison of streamwise vorticity

actively the near inner bank than the outer bank in meandering channel. Therefore, special attentions are paid for the construction of inner bank in meandering channel flow.

3.2 Comparison of Turbulence Results

Figure 6 shows the comparison of turbulent energy normalized by mean frictional velocity $\overline{U_*}$ which is derived by using the value of pressure gradient as well as the experiment. Compared with the experiment at $\theta = -60°$, although the high intensity of turbulent energy is observed both near free surface of central region and inner bank in both results, the present method has a tendency to underpredicts its value. The active production of turbulent energy near inner bank is bound up with the location of maximum streamwise velocity, i.e., the large value of velocity gradient gives rise to promote the turbulent energy near the inner wall. From the experimental results at $\theta = -30°$ and $-0°$, the high intensity of turbulent energy near free surface moves towards the inner bank with the developing flow. This phenomenon is also reproduced by the present calculation and contrary to

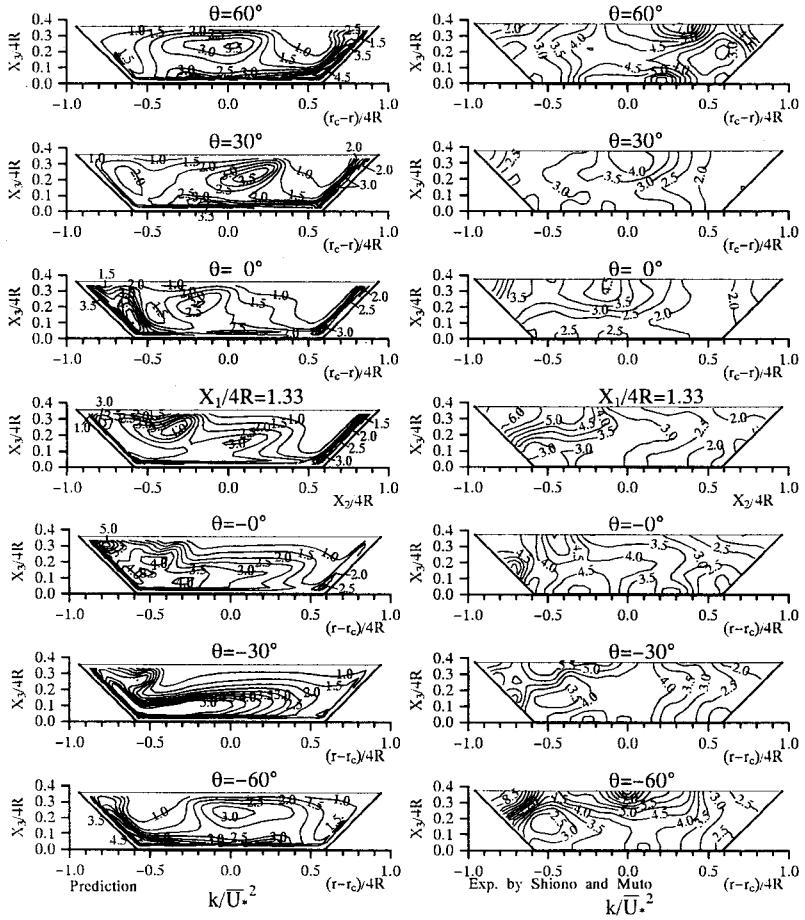

Fig.6: Comparison of turbulent energy

the movement of maximum streamwise velocity from inner bank to outer bank. At $X_1/4R = 1.33$ in straight open channel, the calculation predicts the maximum intensity near free surface in the left hand side of the cross section, while the experiment shows the same tendency of the calculation.

In the second curved channel, the maximum intensity near free surface of central region at $\theta = 0°$ shifts toward inner bank with developing flow in the experimental result. In calculation, the movement of the maximum intensity are observed as a common feature but it is pointed out as a discrepancy that the calculated result at $\theta = 0°$ shows the maximum intensity near the inner bank. Although agreement is certainly not perfect in all detail, the main features are reproduced by the present turbulent model.

Comparison of lateral shear stress $\overline{u_\theta u_r}$ normalized by frictional velocity is shown in figure 7. The different sigh region of shear stress $\overline{u_\theta u_r}$ divided by the zero line is observed in all stations. The zero line of the experiment shifts from inner bank of the first curved channel to inner bank of the second curved channel, while the present method predicts its tendency but does not reproduce the location of zero line preciously. This movement of zero line correlates closely with the movement of

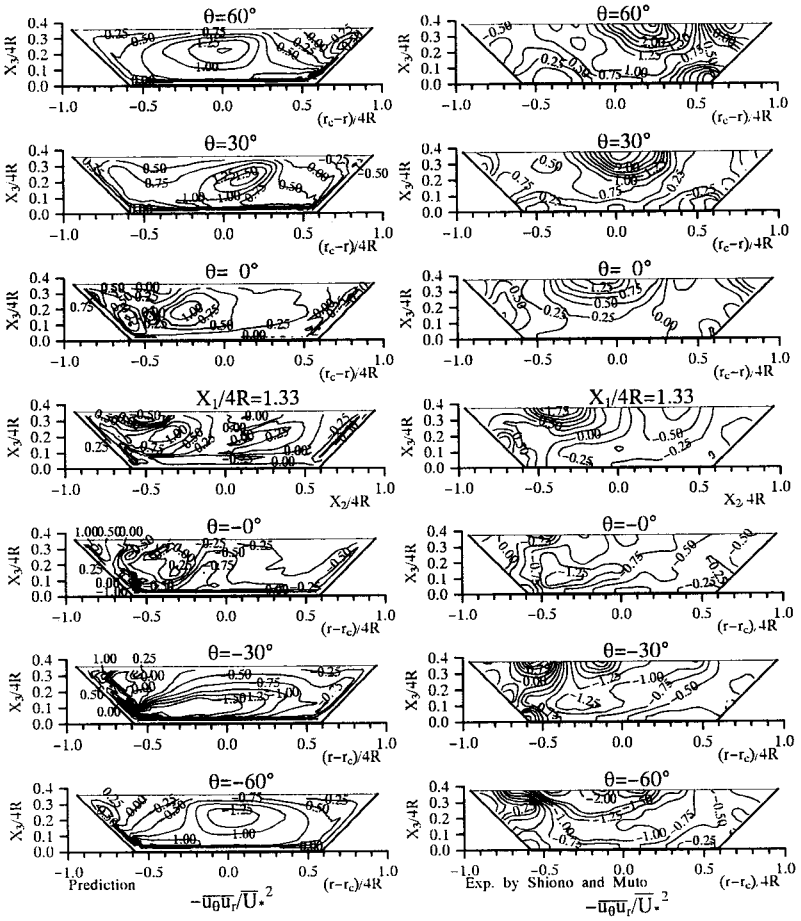

Fig.7: Comparison of lateral shear stress

streamwise velocity as shown in figure 3. The high absolute value of shear stress lies not only near inner bank but also near free surface in both results. This fact suggests that the momentum transfer between streamwise velocity fluctuation and radial velocity fluctuation is promoted actively even near free surface.

Figure 8 shows the comparison results of vertical shear stress $\overline{u_\theta u_z}$ normalized by frictional velocity. As for the shape of zero line, it is different from that of shear stress $\overline{u_\theta u_r}$,i.e., that of shear stress $\overline{u_\theta u_z}$ paralleled with river bed has a tendency to form between inner bank and outer bank, while that of shear stress $\overline{u_\theta u_r}$ is drawn between free surface and river bed. In both results, the maximum absolute intensity is produced near river bed, where the bed generated turbulence is dominated, and the high intensity with negative sigh is observed above the half depth, which the momentum exchange taken place from a bottom layer to an upper layer is dominated. The calculated results suggest that the high intensity of vertical shear stress shifts from the inner bank of the first curved channel to inner bank of the second curved channel with developing flow.

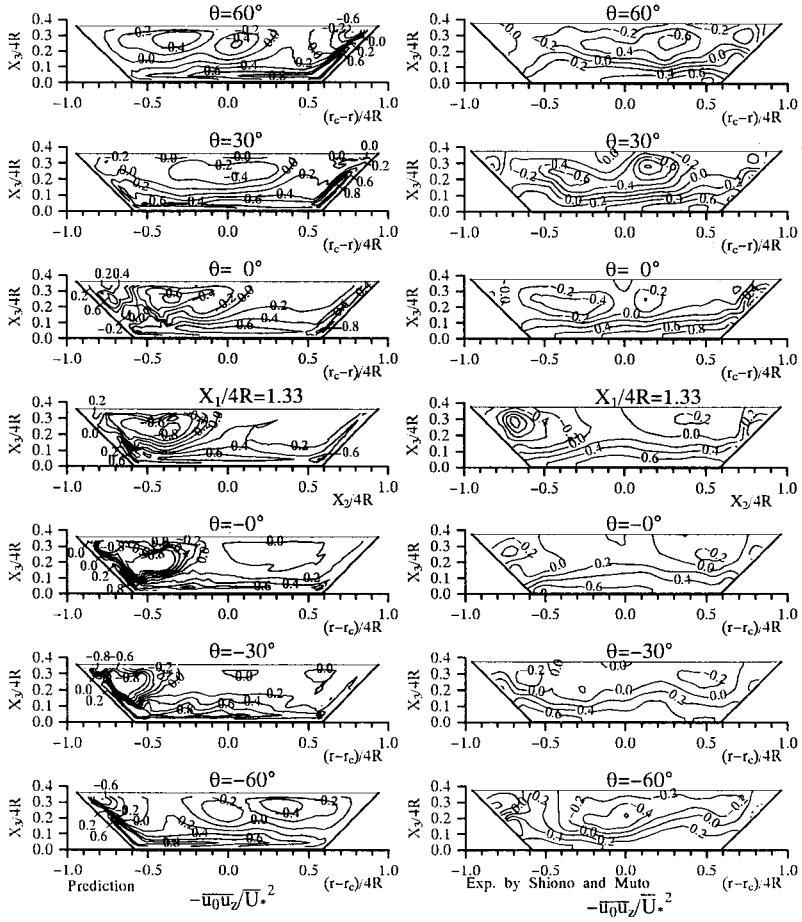

Fig.8: Comparison of vertical shear stress

Further insight into the turbulent structure of meandering channel can be given by examining the data through the invariant of anisotropic tensor. Invariant analysis is based on the concept of physical realizability limits of turbulence which has been used extensively to study the return to isotropy of homogeneous turbulence. Three kinds of invariant tensor which must satisfy the Caley-Hamilton theorem are defined as following equations:

$$I = b_{ij} \tag{9}$$

$$II = -\frac{1}{2} b_{ij} b_{ji} \tag{10}$$

$$III = \frac{1}{3} b_{ij} b_{jk} b_{ki} \tag{11}$$

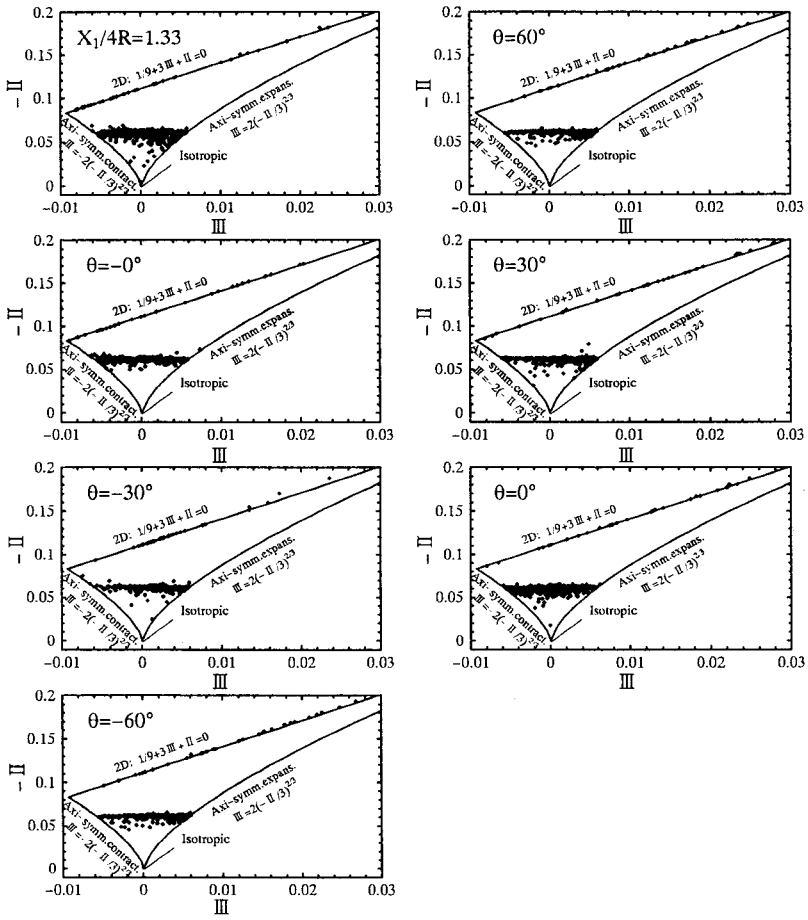

Fig.9: Calculated results of invariant maps

where the anisotropic stress tensor which is first proposed by Rotta [20] is written as follows:

$$b_{ij} = \frac{\overline{u_i u_j} - \frac{2}{3}k\delta_{ij}}{2k} \tag{12}$$

The first invariant I is identically zero by definition of the turbulence kinetic energy. The positive value of third invariant III indicates that there is only one principle components that is large, and a negative value indicates that two principle components are large.

The invariant maps at the same stations of the experiment are derived by using calculated results as shown in figure 9. It is noted that several points are scattered along the 2D line identified two dimensional turbulence in all stations, which phenomenon is caused by the existence of the free surface and , in another words, it is induced by setting the value of velocity fluctuation perpendicular to the free surface to be zero at not only free surface but also the first grid point from the free surface as a boundary condition. These calculated results mean that experimental data are also dotted near the 2D line. In

the curved channel, many points except for points plotted 2D line lie between axi-symmetric line and axi-symmetric expansion line which suggests that the flow is structured anisotropic turbulence. In the straight channel at $X_1/4R = 1.33$, points are scatted more wider than invariants map of curved channel and some points exist near isotropic region. These results indicate that turbulent structure changes partially from anisotropic turbulence to isotropic turbulence. It is noted as a another characteristic feature that invariant map at $\theta = -60°$ is the same that of $\theta = 60°$ as well as streamwise velocity and Reynolds stresses.

4 CONCLUSIONS

Numerical analysis has been carried out for developing turbulent flow in a meandering channel with trapezoidal cross section. In order to predict preciously anisotropic turbulence in this complicated flow, algebraic Reynolds stress model coupled with boundary-fitted coordinate system is adopted in this study. The calculated results are compared with the experimental data available to confirm the validity of the present method and the turbulent structure is examined by introducing invariant analysis. The three mean velocity components, the three Reynolds stress components were compared with the experiment. The conclusions in this research summarized as follows.

As for the comparison of streamwise velocity contours, the present method could predict the characteristic features displaying the movement of maximum velocity from inner bank of the first curved channel to inner bank of the second curved channel and reproduce quantitatively the experimental data. This movement of maximum velocity is bound up with the secondary flow.

At $\theta = -60°$, anti-clockwise vorticity is generated and is seems to prevent maximum velocity from moving towards outer bank in the experiment. This anti-clockwise circulation at $\theta = -60°$ becomes weak as it goes along downstream and disappears before reaching $\theta = -30°$. Entering into the second curved channel, the pressure gradient produces the secondary flow from outer bank to inner bank along river bed. In the experiment at $\theta = 0°$, it is pointed out as a characteristic features that secondary vector near $(r_c - r)/4R = -0.5$ rises up toward the free surface. The present method was able to predict these features well as well as the experiment but the magnitude of the secondary flow evaluated by streamwise vorticity was different from the experiment at a few cross sections.

With regard to comparison of turbulent energy in the experiment, the high intensity of turbulent energy near free surface moves towards the inner wall in the first curved channel with developing flow, which is contrary to the movement of maximum streamwise velocity from inner bank to outer bank. This phenomenon was also reproduced by the present turbulent model.

The high absolute value of lateral shear stress lies not only near inner bank but also near free surface in both experiment and calculation. This phenomenon suggests that the momentum transfer between streamwise velocity fluctuation and radial velocity fluctuation is promoted actively even near free surface. On the other hand, the maximum absolute intensity of vertical shear stress is produced near river bed, where the bed generated turbulence is dominated. Although the calculated results of shear stresses qualitatively agree with these features, that of shear stresses are quantitatively a little different from it.

As a results of comparison with the experiment, it is most likely concluded that the algebraic Reynolds stress model linked with boundary fitted coordinate system is applicable to the meandering open channel flow identified as a complicated three dimensional turbulent flow.

Acknowledgment

The authors would like to express their appreciation to Professor K. Shiono (Loughborough University) and Dr. Y. Muto(Kyoto University), who kindly allowed us to use their experimental results and also provide us valuable suggestions and discussions on this numerical analysis.

REFERENCES

[1] G.H.Toebes and A.A. Sooky (1967) Hydraulics of meandering rivers with flood plains; Proc. ASCE,vol.93 no.ww2 pp.213–236

[2] G.Kiely (1990) Overbank flow in meandering compound channels,The important mechanisms; Int. Conf. on River Flood Hydraulics, pp.207-217

[3] B.B. Willetts and R.I. Hardwick(1993) Stage dependency for overbank flow in meandering channels; Proc. ICE. Wat.,Marit. and Energy, 101 pp.45-54

[4] R.H.J. Sellin, D.A. Ervine and B.B. Willetts (1993) Behaviour of meandering two-stage channels; Proc. ICE. Wat.,Marit. and Energy,101 pp.99-111

[5] D.A. Ervine, B.B. Willetts, R.H.J. Sellin and M. Lorena(1993) Factors affecting conveyance in meandering compound flows; J. Hydraulic Eng., ASCE, vol.119 no.12 pp.1383-1399

[6] K.Shiono and Y.Muto (1993) Secondary flow structure for inbank and overbank flow in trapezoidal meandering compound channel; Proc. 3rd Symp. on Refined Flow Modelling and Turbulence Measurements, pp.645-652

[7] D.A. Ervine and J. Ellis (1987) Experimental and computational aspects of overbank floodplain flow; Transactions of the Royal Society of Edinburgh, 78 pp.315-325

[8] R.K. Greenhill and R.H.J. Sellin (1993) Development of a simple method to predict discharges in compound meandering channels; Proc. ICE. Wat.,Marit. and Energy,101 pp.37-44

[9] Y.Muto, K.Shiono, H.Imamoto and T.Ishigaki (1995) A study on the flow in compound meandering channels; Annuals, Disas. Prev. Res. Inst., Kyoto Univ.,(in Japanese) no.38 B-2 pp.561-580

[10] W. Rodi (1976) A new algebraic relation for calculating the Reynolds stresses; Z.Angew. Math. Mech.,vol.56 pp.T219-T221

[11] H.Sugiyama, M.Akiyama, K.Yamanaka and M.Hirata (1995) Numerical analysis of turbulent structure in a rectangular duct with sand ridges; Computational Fluid Dynamics JOURNAL, vol.4, no.1 pp.59-78

[12] J.C.R.Hunt (1984) Turbulent structure and turbulent diffusion near gas-liquid interfaces; Gas transfer at water surfaces, Reidel Pub., pp.67-82

[13] D.Naot, and W.Rodi (1982) Calculation of secondary currents in channel flow; J. Hydraulics Div.,ASCE., vol.108 pp.948-968

[14] I.Nezu, and H.Nakagawa (1987) Numerical calculation of turbulent open-channel flows by using a modified $k-\epsilon$ turbulence model; Proc. of Japan Soc. Civil Engrs., (in Japanese) vol.387 pp.125-134

[15] H.Nakagawa, I.Nezu, and H.Ueda (1975) Turbulence of open channel flow over smooth and rough beds; Proc.of Japan Soc. Civil Engrs., vol.241 pp.155-168

[16] H.Sugiyama, M.Akiyama, T.Matsubara and M.Hirata (1995) Numerical analysis of three-dimensional turbulent structure in open channel flow; Computational Fluid Dynamics JOURNAL,vol.4, no.2 pp. 239-262

[17] H.Sugiyama, M.Akiyama, M.Matsumoto, M.Hirata, and N.Ninomiya (1993) Numerical analysis of fully developed turbulent flow in a square duct with two facing roughened walls; Computational Fluid Dynamics JOURNAL, vol.2, No.3 pp.319-338

[18] B.P.Leonard (1979) A stable and accurate convective modelling procedure based on quadratic upstream interpolation; Comp. Meths. Appl. Mech. Eng., vol.19 pp.59-98

[19] Y.Shimizu, Y.Futaki and C.S. Martin (1992) Secondary flow and Hydraulic losses within sinuous conduits of rectangular cross section; Transactions of the ASME, J. of Fluid Engineering, vol.114 pp.593-600

[20] J.C.Rotta (1951) Statistische theorie nichthomogener turbulenz; Mitteilung-Zeitschrift für Physik, vol. 129 pp.547-572